4. Muxi A, Sola M, Bassa P, et al. Radioimmunoscintigraphy of colorectal carcinoma with a ^{99m}Tc-labelled anti-CEA monoclonal antibody (BW431/26). *Nucl Med Commun* 1992;13:261–270.
5. Gallup DG Maguire RT, Van Nostrand D, eds. *Diagnosis of colorectal and ovarian carcinoma: Application of immunoscintigraphic technology.* New York: Marcel Dekker, 1992. Multicenter clinical trial of ^{111}In-CYT-103 in patients with ovarian cancer.
6. Merino MJ, Monteagudo C, Neumann RD. Monoclonal antibodies for radioimmunoscintigraphy of breast cancer. *Nucl Med Biol* 1991;18:437–443.
7. Lind P, Sola M, Leichner P, et al. The immunoscintigraphic use of Technetium-99m labelled monoclonal anti-CEA antibodies (BW 431/26) in patients with suspected primary, recurrent and metastatic breast cancer. *Int J Cancer* 1991;47:865–869.
8. Murray JL, Rosenblum MG, Lamki L, et al. Clinical parameters related to optimal tumor localization of indium-111-labeled mouse antimelanoma monoclonal antibody ZME-018. *J Nucl Med* 1987;28:25–33.
9. Lamberts SWJ, Reubi J, Krenning EP. Somatostatin and the concept of peptide receptor scintigraphy in oncology. *Semin Oncol* 1994;21:1–5.
10. Krenning EP, Kwekkeboom DJ, Bakker WH, et al. Somatostatin receptor scintigraphy with ^{111}In-DTPA-D-Phe^{1}and ^{23}I-Tyr^3-octreotide: the Rotterdam experience with more than 1000 patients. *Eur J Nucl Med* 1993;20:716–731.
11. Van Eijck CHJ, Krenning EP, Bootsma A, et al. Somatostatin-receptor scintigraphy in primary breast cancer. *Lancet* 1994;343:640–643.
12. Sainsbury JRC, Farndon JR, Sherbet GV, Harris AL. Epidermal growth factor receptors and oestrogen receptors in human breast cancer. *Lancet I* 1985;8425:364–366.
13. Rios MA, Macias A, Perez R, et al. Receptors for epidermal growth factor and estrogen as predictors of relapse in patients with mammary carcinoma. *Anticancer Res* 1988;8:173–176.
14. Fitzpatrick SL, Brightwell J, Wittliff JL, et al. Epidermal growth factor binding to breast tumor biopsies and relationship to estrogen receptor and progestin receptor levels. *Cancer Res* 1984;44:3448–3453.
15. Nicholson S, Sainsbury JRC, Needham GK, et al. Quantitative assays of epidermal growth factor receptor in human breast cancer: cutoff points of clinical relevance. *Int J Cancer* 1988;42:36–41.
16. Motulsky HJ. GraphPad prism ver. 1.0. San Diego: GraphPad Software Inc., 1995.
17. McEwan AJB, MacLean GD, Hooper HR, et al. MAb 170H0.82: an evaluation of a novel panadenocarcinoma monoclonal antibody labelled with ^{99m}Tc and with ^{111}In. *Nucl Med Commun* 1992;13:11–19.
18. Collier BD, Abdel-Nabi HH, Doerr RJ, et al. Immunoscintigraphy performed with Indium-111 labeled CYT-103 in the management of colorectal cancer: comparison with CT. *Radiology* 1992;185:179–186.
19. Abdel-Nabi H, Doerr RJ, Evans NH, et al. Radioimmunodetection of colorectal carcinoma with ^{111}In-labelled monoclonal antibody IVPZCE 025 (a tissue culture produced anti-CEA MAb). *Nucl Med Commun* 1994;15:81–93.
20. Maini CL, Sciuto R, Tofani A, et al. Somatostatin receptor imaging in CNS tumours using ^{111}In octreotide. *Nucl Med Commun* 1995;16:756–766.
21. Muraro R, Frati L, Bei R, et al. Regional heterogeneity and complementation in the expression of the tumor-associated glycoprotein 72 epitopes in colorectal cancer. *Cancer Res* 1991;51:5378–5383.
22. Reubi JC, Waser B, Foekens JA, et al. Somatostatin receptor incidence and distribution in breast cancer using receptor autoradiography: relationship to EGF receptors. *Int J Cancer* 1990;46:416–420.
23. Carrasquillo JA, Abrams PG, Schroff RW, et al. Effect of antibody dose on the imaging and biodistribution of indium-111 9.2.27 antimelanoma monoclonal antibody. *J Nucl Med* 1988;29:39–47.
24. Cuartero-Plaza A, Martinez-Miralles E, Rosell R, et al. Radiolocalization of squamous lung carcinoma with ^{131}I-labeled epidermal growth factor. *Clin Cancer Res* 1996;2:13–20.
25. Griffin TW, Bokhari F, Collins J, et al. A preliminary pharmacokinetic study of ^{111}In-labeled 260F9 anti-(breast cancer) antibody in patients. *Cancer Immunol Immunother* 1989;29:43–50.
26. Lakshmanan AV, Sharp P, Mallard J. The influence of size and radiopharmaceutical concentration ratio on the detection of abnormalities in clinical radionuclide imaging. *Br J Radiology* 1978;51:986–991.
27. Rockoff SD, Goodenough DJ, McIntire KR. Theoretical limitations in the immunodiagnostic imaging of cancer with CT and nuclear scanning. *Cancer Res* 1980;40:3054–8.
28. Kuo B, Kusmik WF, Poole JC, et al. Pharmacokinetic evaluation of two human epidermal growth factors (hEGF51 and hEGF53) in rats. *Drug Metab Dispos* 1992;20:23–30.
29. Kim DC, Sugiyama Y, Fuwa T, et al. Kinetic analysis of the elimination process of human epidermal growth factor (hEGF) in rats. *Biochem Pharmacol* 1989;38:241–249.
30. Carbone PP, Jordan VC, Bonadonna G, Calabresi P, Schein PS, eds. *Medical oncology: Basic principles and clinical management of cancer.* Toronto: McGraw-Hill, Inc., 1993: 819–849.
31. Dunn WA, Hubbard AL. Receptor-mediated endocytosis of epidermal growth factor by hepatocytes in the perfused rat liver: ligand and receptor dynamics. *J Cell Biol* 1984;98:2148–2159.
32. Colcher D, Bird R, Roselli M, et al. In vivo tumor targeting of a recombinant single-chain antigen-binding protein. *J Natl Cancer Inst* 1990;82:1191–1197.
33. Tan P, Bailey DL, Meikle SR, Eberl S, Fulton RR, Hutton BF. A scanning line source for simultaneous emission and transmission measurements in SPECT. *J Nucl Med* 1993;34:1752–1760.

Kinetic Analysis of 2-[Carbon-11]Thymidine PET Imaging Studies: Compartmental Model and Mathematical Analysis

David A. Mankoff, Anthony F. Shields, Michael M. Graham, Jeanne M. Link, Janet F. Eary and Kenneth A. Krohn

Division of Nuclear Medicine, University of Washington, Seattle, Washington; and Wayne State University and the Karmanos Cancer Institute, Detroit, Michigan

Carbon-11-thymidine is a PET tracer of DNA synthesis and cellular proliferation. Quantitative analysis of [^{11}C]thymidine images is complicated by the presence of significant quantities of labeled metabolites. Estimation of the rate of thymidine incorporation into DNA using [^{11}C]thymidine requires a kinetic model that is capable of describing the behavior of thymidine and labeled metabolites. **Methods:** Based on previous studies with labeled thymidine, we constructed a five-compartment model describing the kinetic behavior of 2-[^{11}C]thymidine and its labeled metabolites. In addition, we have performed a series of calculations and simulations to calculate the sensitivity and identifiability of model parameters to estimate the extent to which individual parameters can be estimated; to determine appropriate model constraints necessary for reproducible estimates of the constant describing flux of thymidine from the blood into DNA, i.e., thymidine flux constant; and to determine the potential accuracy of model parameter and thymidine flux constant estimates from PET imaging data. **Results:** The underlying assumptions in the thymidine compartmental model lead to a description of the thymidine flux constant for DNA incorporation in terms of model parameters. Sensitivity and identifiability analyses suggest that the model parameters pertaining to labeled metabolites will be difficult to estimate independently of the thymidine parameters. Exact evaluation of the kinetic parameters of the labeled metabolites is not the principal goal of this model. Simulations were performed that suggest that it is preferable to tightly constrain these parameters to preset values near the center of their expected ranges. Although it is difficult to estimate individual thymidine model parameters, the flux constant for incorporation into DNA can be accurately estimated ($r > 0.9$ for estimated versus true simulated flux constant). Flux constant estimates are not affected by modest levels of local degradation of thymidine that may occur in proliferating tissue. **Conclusion:** By using a kinetic model for thymidine and labeled metabolites, it is possible to estimate the flux of thymidine uptake and incorporation into DNA and, thereby, noninvasively estimate regional cellular proliferation using [^{11}C]thymidine and PET.

Key Words: PET; carbon-11-thymidine; kinetic modeling; cancer

J Nucl Med 1998; 39:1043–1055

Received Apr. 1, 1997; revision accepted Aug. 14, 1997.

For correspondence or reprints contact: David A. Mankoff, MD, PhD, Division of Nuclear Medicine, Box 356113, University of Washington Medical Center, 1959 NE Pacific St., Seattle, WA 98195.

Labeled thymidine has been used extensively to measure DNA synthesis rates and cell cycle kinetics (*1*). One application has been in tumor biology, where labeled thymidine uptake has been used to measure cellular proliferation (*1–8*). These studies have been largely performed in vitro in tumor cell lines or in animal tumor models in a limited number of in vivo studies (*2,3*). Labeled thymidine studies of cells cultured from biopsied or resected tumors have been used to characterize the proliferation of individual human tumors for several cancer types (*4,8*), and growth studies of cells exposed to various chemotherapeutic agents have been used to predict response to chemotherapy (*5,9*). Although these approaches have met with some success, in vitro studies of biopsied tumors are limited by the significant heterogeneity of tumors and the subsequent sampling error, as well as the inability of in vitro studies to account for all in vivo factors that affect tumor growth and response to therapy, such as host-tumor interactions and chemotherapeutic agent metabolism (*9*).

Carbon-11-thymidine has been developed and tested as a PET tracer of thymidine incorporation into DNA and, thus, of tissue proliferation (*6,10–14*). Preliminary studies have demonstrated the potential for this tracer to measure tumor proliferation and response to therapy (*15,16*). The analysis of thymidine PET images, however, is complicated by the fact that the tracer is rapidly metabolized (*17,18*), first by the enzymatic cleavage of the sugar and then reduction and ring opening. Much of the ^{11}C label imaged in thymidine studies is in the form of labeled metabolites, which are not part of the biochemical pathway by which thymidine is incorporated into DNA (*17–20*). To use dynamic PET imaging to estimate the rate of [^{11}C]thymidine incorporation into DNA, a kinetic model is required that realistically describes the biochemistry of thymidine incorporation into DNA and accounts for the contribution of labeled metabolites. The goal of such analysis is to use dynamic PET images to estimate the thymidine incorporation rate, i.e., the flux of labeled thymidine from the blood into tissue DNA.

Toward this goal, our laboratory has studied the in vivo behavior of [^{11}C]thymidine in animals and patients (*11,17,19–21*). We have developed methods for measuring labeled metabolites in the blood at various times after injection (*17*). We have also studied uptake and metabolism of thymidine labeled in the methyl position compared to the ring-2 position (*12,14,19*) (see Fig. 1 for chemical structure). These studies showed that there are fewer labeled metabolites when the ring-2 position is labeled and that the metabolites are less likely to be trapped in tissue and mistaken for labeled thymidine incorporated into DNA (*19*).

In this article, we present a compartmental model for 2-[^{11}C]thymidine and review evidence from the literature and our preliminary studies that tests the validity of the model. We also present calculations and simulations that test the ability of the model to estimate thymidine flux into DNA, given the quality of the data that would be expected in a typical [^{11}C]thymidine PET study. Finally, we present an example of analysis of PET studies in a patient imaged before and after one cycle of chemotherapy. In a separate report, we will describe in vivo experiments performed to further characterize model parameters and to test the validity of the model's predictions of labeled thymidine incorporation.

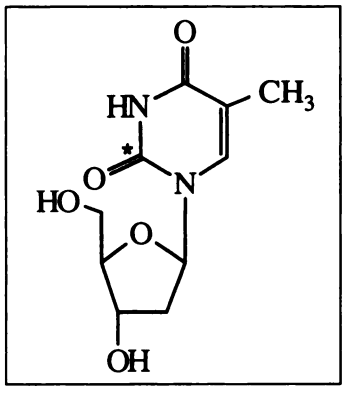

FIGURE 1. Chemical structure of thymidine showing labeling position for 2-[^{11}C]thymidine (asterisk).

BACKGROUND AND THEORY

General Considerations

2-[Carbon-11]thymidine is being evaluated as a tracer of the external or salvage pathway of thymidine incorporation into DNA. In this pathway, thymidine that is external to the cell, as opposed to thymidine synthesized de novo, is incorporated into DNA (*1*). Through kinetic analysis of 2-[^{11}C]thymidine images, it should be possible to infer thymidine flux through this pathway as a measure of tumor proliferation. We show that the assumptions in our model lead to a form in which the flux of thymidine from the blood into DNA ($Flux_{TdR}$, in μmol/min/g) can be described by the product of the native (unlabeled) thymidine blood concentration ($[TdR]_b$, in μmol/ml) and a flux constant (K_{TdR}, in ml/min/g):

$$Flux_{TdR} = [TdR]_b \cdot K_{TdR}. \qquad \text{Eq. 1}$$

In the discussion that follows, we describe the relationship of K_{TdR} to compartmental model parameters and show how K_{TdR} can be estimated using data obtained in a dynamic [^{11}C]thymidine PET study.

The external pathway provides only a fraction of the thymidine used in DNA synthesis, with the remainder provided by the de novo pathway (*1*). We have previously shown that the fraction of thymidine incorporated into DNA through the external pathway (f_{ext}) is a function of the concentration of thymidine in the extracellular fluid (*21*). Thymidine is readily permeable through somatic tissue capillaries (*1,22*), and the extracellular fluid concentration should, therefore, be closely related to the blood concentration. Thus, if the thymidine blood concentration is known, the DNA synthetic rate (SR_{DNA}) in the tumor can, in principle, be calculated from measurements of the flux through the external pathway, scaled to account for DNA synthesis that uses thymidine from the de novo pathway:

$$SR_{DNA} = 2 \cdot \frac{1}{f_{ext}} \cdot Flux_{TdR}$$

$$= 2 \cdot \frac{1}{f_{ext}} \cdot [TdR]_b \cdot K_{TdR}. \qquad \text{Eq. 2}$$

The factor of 2 arises from the fact that approximately one-half of the DNA base pairs contain thymidine (*1*).

The possible fates of intravenously administered thymidine in vivo are illustrated in Figure 2 (*1*). In addition to the incorporation pathway, in which thymidine is phosphorylated and incorporated into DNA, thymidine can be degraded by thymidine phosphorylase to thymine and then reduced to dihydrothymine (DHT) and then to β-ureidoisobutyric acid (BUIB) and β-aminoisobutyric acid. For thymidine labeled at the ring-2 position, degradation products beyond BUIB do not contain the label, which leaves the pathway as [^{11}C]CO_2. Degradation takes place rapidly in the liver and blood, and labeled metabolites appear in significant quantities in the blood within minutes after injection (*17*) (see example in Fig. 3). Thus, to estimate thymidine flux from the blood into DNA,

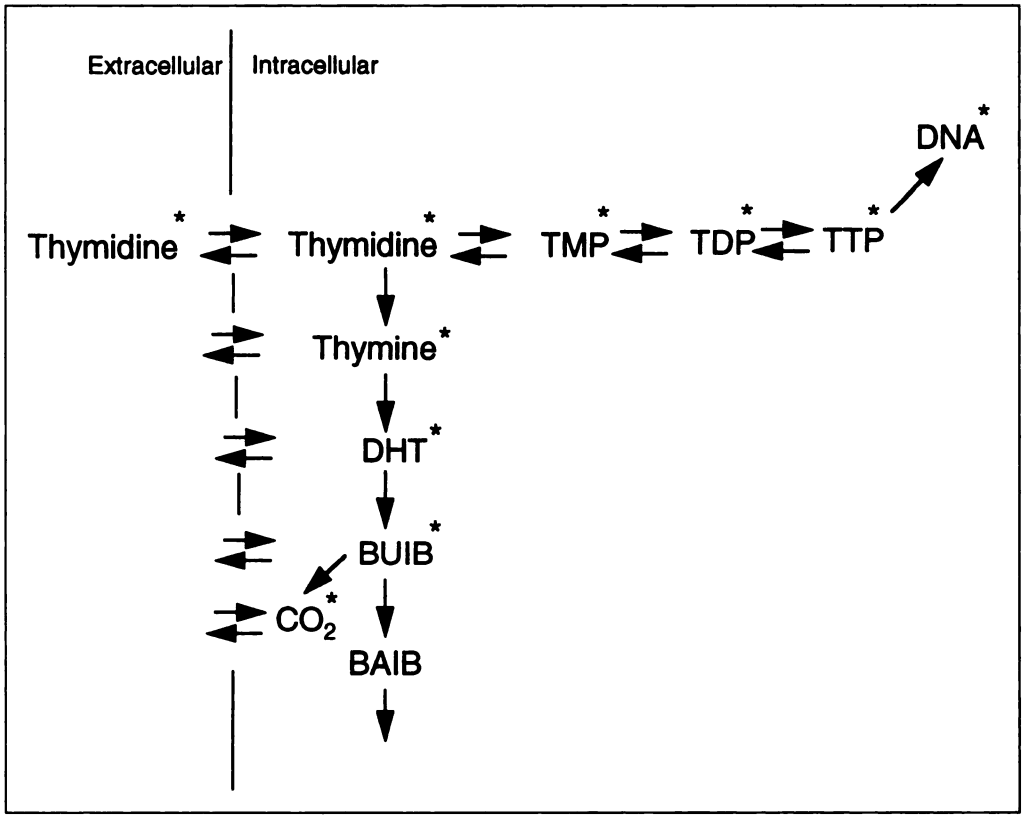

FIGURE 2. Possible fates of thymidine in vivo. Pathway to incorporation into DNA is shown proceeding left to right; degradative pathway is shown proceeding downward. Asterisk indicates labeled compound for thymidine labeled in the ring-2 position. BAIB = β-aminoisobutyric acid; TMP = thymidine monophosphate; TDP = thymidine diphosphate; DHT = dihydrothymine; BUIB = β-ureidoisobutyric acid.

kinetic analysis must separate the contribution of labeled metabolites to the total tissue activity in dynamic PET imaging from that of intact [^{11}C]thymidine. For methyl-labeled thymidine, labeled degradation products beyond BUIB can become incorporated into molecules trapped in cells, and it is more difficult to separate the contribution of trapped labeled metabolites from labeled thymidine incorporated into DNA (*19,23*). We have therefore chosen to model the ring-2 [^{11}C]thymidine (*12,14*).

Model

The kinetic model for 2-[^{11}C]thymidine is illustrated in Figure 4. Three separate compartment sets are driven by three separate blood input functions obtained from metabolite analysis of blood samples. Whole-blood measurements are used for the blood inputs. Because the transport of thymidine across the red cell membrane is rapid and the thymidine distribution volume in the red cell is nearly the red cell water space (*24*), whole blood serves as an appropriate input for thymidine. For the metabolites, inclusion of the red cells in measurements of whole blood might cause errors if the concentration in the red cell were significantly different from the plasma. The compartment sets describe the kinetic behavior of [^{11}C]thymidine, [^{11}C]CO_2 and a group of labeled small molecules ("metabolites") that includes [^{11}C]thymine, [^{11}C]DHT and [^{11}C]BUIB. The tissue thymidine compartment (A) represents all species encountered along the external pathway between the time thymidine leaves the blood until it is incorporated into DNA (B). As discussed below, the model assumes that the rate-limiting steps for thymidine in the blood to be incorporated into DNA are blood-to-tissue transit and thymidine triphosphate (TTP) incorporation into DNA. Therefore, the thymidine tissue compartment includes intracellular thymidine and thymidine nucleotides, often referred to as the thymidine DNA precursor pool (*1*). The tissue metabolite compartment (C) represents labeled thymine, DHT and BUIB, which are assumed to have only reversible transport into tissue. The tissue CO_2 compartment (D) represents labeled CO_2 and HCO_3^- reversibly transported into tissue, whereas the fixed CO_2 compartment (E) represents labeled CO_2 that has become incorporated into molecules that are trapped in tissue over the time course of the study.

By using the notation illustrated in Figure 4, the following differential equations characterize the compartmental model. The tracer content in the tissue compartments (A–E) is expressed in units of activity per gram of tissue (μCi/g) (units for the other variables are given in the Appendix):

$$\frac{dA}{dt} = K_{1t}[TdR]_b - (k_{2t} + k_{3t})A, \quad \text{Eq. 3}$$

$$\frac{dB}{dt} = k_{3t}A, \quad \text{Eq. 4}$$

$$\frac{dC}{dt} = K_{1m}[Met]_b - k_{2m}C, \quad \text{Eq. 5}$$

$$\frac{dD}{dt} = K_{1c}[CO_2]_b - (k_{2c} + k_{3c})D, \quad \text{Eq. 6}$$

$$\frac{dE}{dt} = k_{3c}D. \quad \text{Eq. 7}$$

The sum of all tissue compartments plus activity in the blood volume contained within the tissue combine to form the total tissue activity, which is measured on a regional basis in the dynamic PET study:

$$\text{Tissue total tracer content} = A + B + C + D + E + V_b([TdR]_b + [Met]_b + [CO_2]_b). \quad \text{Eq. 8}$$

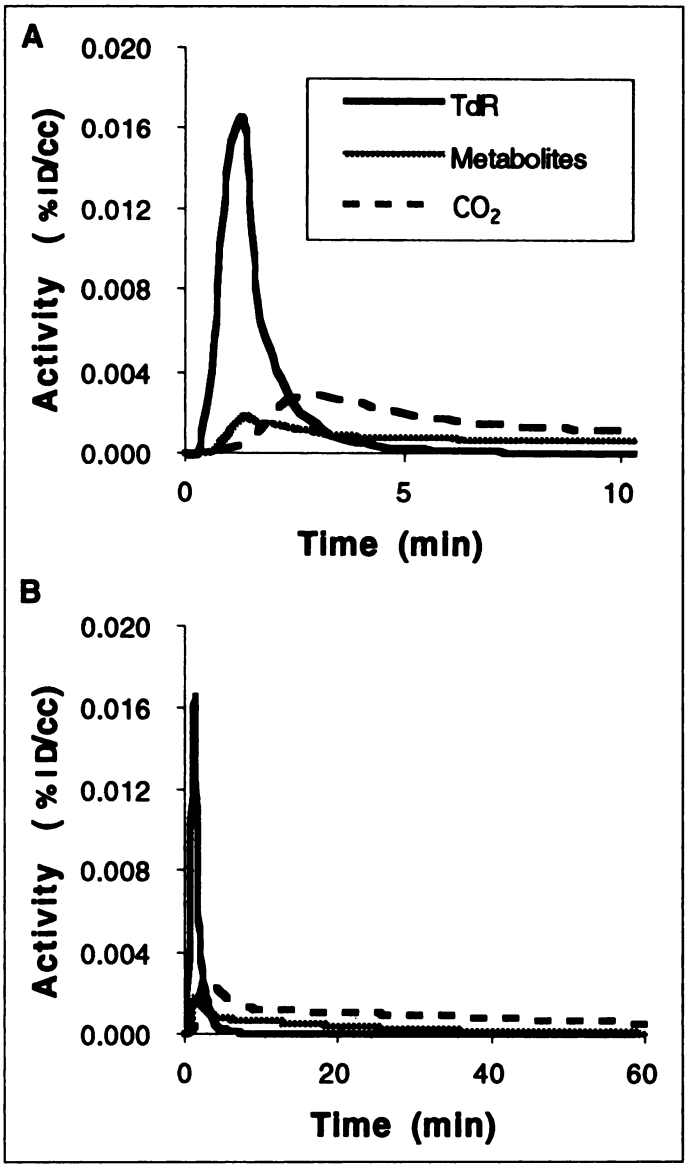

FIGURE 3. Time course of thymidine and labeled metabolites [CO_2 and non-CO_2 metabolites ("metabolite") groups] in the blood for a typical patient study. Smoothed curves are shown for clarity. (A) Expanded view of time-activity curves for first 10 min after injection. (B) Time-activity curves over 60 min after injection.

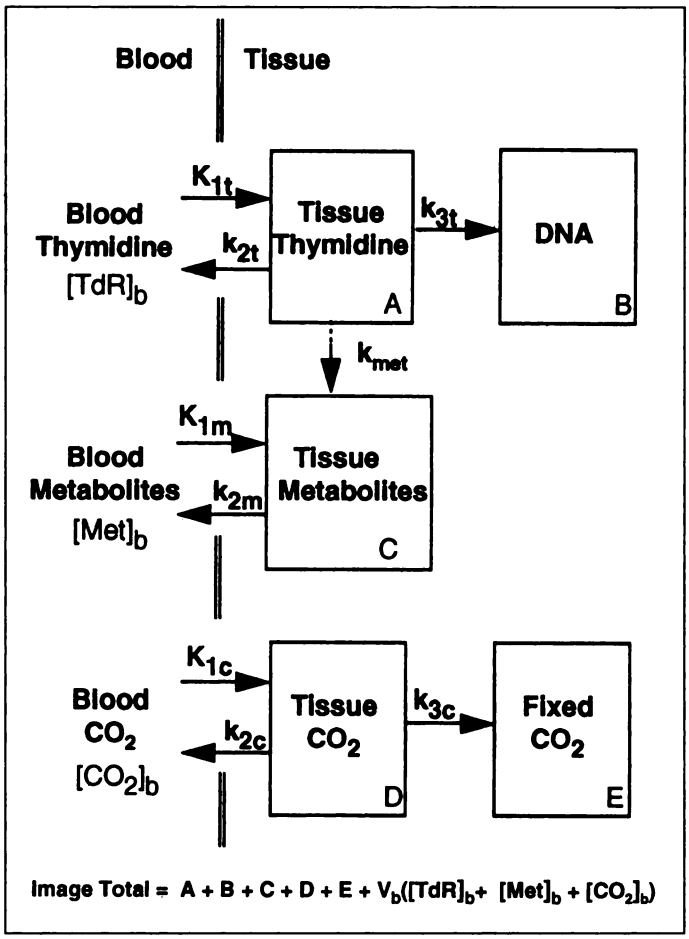

FIGURE 4. Compartmental model for 2-[^{11}C]thymidine. Line labeled k_{met} shows pathway simulated in the test of the effect of local degradation. This pathway was otherwise not used.

The units for total tissue tracer content are μCi/g. This is obtained from the PET image activity concentration divided by the tissue density. For the purposes of this discussion, we have assumed a tissue density of 1 g/ml.

The kinetic model pictured in Figure 4 includes five tissue compartments and eight rate constants to be estimated, given three measured blood input functions (thymidine, metabolites and CO_2) and the total tissue time-activity curve obtained from dynamic PET imaging. In addition to the rate constants, the blood volume (V_b) and relative delay between the blood sampling site and the tissue of interest (Δt) are additional parameters of the model. It seems unreasonable to expect that, given that the three blood input functions have relatively similar time courses and that there is considerable noise inherent in the tissue time-activity curve, we will be able to accurately estimate all 10 model parameters. With this in mind, the model has been pared to its essential elements, and simplifying assumptions have been used wherever possible to reduce the number of variables to be estimated. These assumptions are discussed below.

Model Assumptions

Thymidine Compartment Set

Assumption 1: Thymidine Transport. *Blood flow and capillary transit, represented by the parameter K_1, are the primary barriers to the initial distribution of the tracer in the cell. Transport across cell membranes is sufficiently rapid so as not to be a rate-limiting step.*

Studies of thymidine transport in a variety of cells (*24,25*), including cultured tumor cells and red blood cells, have shown that thymidine transport through the adenosine transporter at physiologic thymidine concentrations has transport rate constants that are much higher than typical blood flow rates and rates of thymidine phosphorylation, the next step in the incorporation pathway (*26*). For example, in the study of Wohlhueter et al. (*25*), Novikoff hepatoma cells, Chinese hamster ovary cells and mouse L cells were found to have Michaelis-Menten membrane transport rate constants of 7–32 μM (K_m) and 103–228 pmol/sec/μl cell water (V_{max}). Blood concentrations of thymidine in humans are typically 1 μM or less (*27*), much lower than K_m, in which case membrane transport rate constants are approximated by V_{max}/K_m. Assuming 0.6 ml of cell water per ml tissue volume, the resulting rate constants for transport across the cellular membrane are in the range of 2.3–6.5 ml/min/g. This rate is greater than blood flow in even the most well-vascularized tumor (*28,29*). Thus, blood flow and capillary permeability, rather than cellular membrane transport, will limit thymidine transport to tissues.

This assumption allows us to model thymidine delivery to tissue using a single rate constant, K_1. This rate constant will be a

function of tissue blood flow and capillary permeability to thymidine and has units of ml/min/g.

Assumption 2: Thymidine Incorporation into DNA. *Once tracer is delivered to the tissue, the rate-limiting step for insertion into DNA is the incorporation of TTP from the precursor pool into DNA. The incorporation of thymidine precursors into DNA can be described by first-order rate constant, k_3. Furthermore, over the time course of imaging, precursor incorporation into DNA is irreversible.*

This assumption stems from the four-factor model of thymidine kinetics proposed by Cleaver (*1*) and Quastler et al. (*7*), which depicts the thymidine precursor pool [intracellular thymidine, thymidine monophosphate (TMP), thymidine diphosphate (TDP) and TTP) as a freely mixing pool common to both the de novo and external pathways and in which TTP incorporation into DNA is the rate-limiting step. This model has been supported by several in vivo tumor studies and in vitro cell culture studies (*2,30–35*), which have shown rapid intracellular uptake of labeled thymidine and generation of TMP, TDP and TTP. In these studies, levels of labeled TTP are higher than any of the other species, suggesting that incorporation of labeled TTP into DNA is the rate-limiting step. Furthermore, studies have shown that over a 1-hr period, label incorporated into DNA is not released (*1*).

Cleaver (*1*), Quastler et al. (*7*) and Colby and Edlin (*36*) have put forth the observation that the rate of native (unlabeled) TTP incorporation into DNA is dependent on the proliferative state of the cell and is not dependent on the concentration of TTP, i.e., that DNA synthesis has zero order dependency on the tissue thymidine concentration and thymidine precursor pool size. Therefore, for labeled thymidine, the rate of labeled TTP incorporation into DNA has first-order dependence on the tissue concentration of labeled thymidine and precursors because the rate of labeled thymidine incorporation into DNA will be dependent on its specific activity in the precursor pool.

It should be noted that the notions of a single thymidine precursor pool and zero-order dependence on the precursor pool for the thymidine DNA incorporation rate are not universally accepted. In particular, some authors have proposed that there are multiple precursor pools rather than a single precursor pool with rapid turnover (*37*). Others have proposed that thymidine delivery to cells or initial phosphorylation of thymidine might be rate-limiting (*15,38,39*). Nevertheless, the preponderance of evidence in rapidly dividing cell lines and tumors supports a single precursor pool with rapid turnover and TTP incorporation into DNA as the rate-limiting step (*1,2,7,30–36*).

The first-order dependence on the tissue thymidine compartment (largely composed of the thymidine precursor pool) of tracer thymidine incorporation into DNA leads directly to a description of the rate constant for thymidine incorporation into DNA (k_{3t}):

Labeled thymidine flux into DNA=

$$k_{3t} \cdot [TdR^*]_{tis} = Flux_{TdR} \cdot \frac{[TdR^*]_{tis}}{[TdR]_{tis}}, \qquad \text{Eq. 9}$$

where $[TdR^*]_{tis}$ and $[TdR]_{tis}$ refer to the labeled and native tissue thymidine and thymidine DNA precursors, respectively (compartment A in Fig. 4), and $Flux_{TdR}$ refers to flux of thymidine into DNA through the external pathway, as in Equations 1 and 2. These equations, therefore, define k_{3t} as:

$$k_{3t} = \frac{Flux_{TdR}}{[TdR]_{tis}}. \qquad \text{Eq. 10}$$

At equilibrium, the content of the tissue TdR compartment (Compartment A, $[TdR]_{tis}$) is constant, and therefore:

$$K_{1t} \cdot [TdR]_b = (k_{2t} + k_{3t}) \cdot [TdR]_{tis}, \qquad \text{Eq. 11}$$

where $[TdR]_b$, as in previous equations, is the concentration of thymidine in the blood. Incorporating this expression into Equation 10 leads to a description of $Flux_{TdR}$ in terms of model parameters:

$$Flux_{TdR} = [TdR]_b \cdot \frac{K_{1t}k_{3t}}{k_{2t} + k_{3t}}. \qquad \text{Eq. 12}$$

By comparison with Equation 1, the ratio of constants on the right side of Equation 12 is defined as the thymidine blood–tissue transfer or flux constant (K_{TdR}), defined by:

$$K_{TdR} = \frac{K_{1t}k_{3t}}{k_{2t} + k_{3t}}. \qquad \text{Eq. 13}$$

The expected range for k_{3t} can be obtained from cellular experiments where specific activity in the DNA precursor pool was measured after unlabeled thymidine was used to "chase" labeled thymidine from the precursor pool of cells that had been previously incubated with labeled thymidine (*1,37,40,41*). Loss of label from the intracellular pool occurs through incorporation into DNA (i.e., k_{3t}) and return of labeled compound to the extracellular fluid (k_{2t}). These experiments therefore provide the expected upper limit on k_{3t} (if washout other than incorporation into DNA was negligible). By estimation of the exponential decay constants from washout curves that have been reported (*1,40,41*), the expected maximum for k_{3t} is in the range of 0.15–0.20 min^{-1}.

Assumption 3: Reversibility of Thymidine Uptake Before TTP Incorporation into DNA. *Labeled thymidine delivered to the tissue can leave the tissue compartment at any point in the external incorporation pathway until labeled TTP is incorporated into DNA. Specifically, label in the form of intracellular thymidine and thymidine nucleotides can leave the cell in the form of thymidine or a degradation product. This allows us to model label in the form of tissue thymidine, TMP, TDP and TTP as belonging to a single, reversible tissue compartment.*

Several studies using chases of cold thymidine after incubation with labeled thymidine show that, even when DNA synthesis is blocked, some or all of the label initially taken up into the cell and appearing as thymidine and nucleotides can washout of cells (*30,31,38,42*). Although the labeled species leaving the cell were not identified, they were most likely thymidine or a degradation product such as thymine because the phosphorylated precursors would be unlikely to cross the cellular membrane (*38,43*).

This assumption, combined with Assumption 2, allows us to model tissue thymidine and thymidine nucleotides as a single compartment with reversible transport, greatly simplifying the model and description of thymidine incorporation into DNA by a flux constant, as described in Equations 1 and 13.

The expected size of the tissue thymidine compartment can be inferred from studies that have measured the concentration of intracellular thymidine and nucleotides (i.e., TMP, TDP and TTP) relative to the incubating medium (*32,34,44*). The ratio of the total label in intracellular small molecules relative to the incubating medium provides an estimate of the virtual volume of distribution of thymidine (V_{TdR}). V_{TdR} is defined by the tissue-to-blood ratio of thymidine concentration:

$$V_{TdR} = \frac{[TdR]_{tis}}{[TdR]_b}, \qquad \text{Eq. 14}$$

where V_{TdR} has units ml/g, $[TdR]_{tis}$ has units μmol/g and $[TdR]_b$ has units μmol/ml. Tissue is composed of extracellular and intracellular space; therefore, $[TdR]_{tis}$ is given by:

$$[TdR]_{tis} = V_{ECF}[TdR]_{ECF} + V_{ICF}([TdR]_{cell} + [TP]_{cell}), \quad \text{Eq. 15}$$

where V_{ECF} and V_{ICF} are the extracellular and intracellular volumes in ml/g, $[TdR]_{ECF}$ and $[TdR]_{cell}$ are the extracellular and intracellular concentrations of thymidine in μmol/ml, and $[TP]_{cell}$ is the total intracellular concentration of thymidine nucleotides in μmol/ml (also considered part of tissue thymidine in compartment A), given by:

$$[TP]_{cell} = [TMP]_{cell} + [TDP]_{cell} + [TTP]_{cell}. \quad \text{Eq. 16}$$

At equilibrium, the concentration of thymidine in the extracellular fluid should be similar to that in the blood because thymidine does not appear to be concentrated across the capillary wall (*1,22*). Therefore, the thymidine concentrations in the blood and extracellular fluid ($[TdR]_b$ and $[TdR]_{ECF}$, respectively) will be nearly the same, and the combination of Equations 14 and 15 results in:

$$V_{TdR} = V_{ECF} + \frac{[TdR]_{cell} + [TP]_{cell}}{[TdR]_{ECF}} \cdot V_{ICF} \quad \text{Eq. 17}$$

$$= V_{ECF} + R \cdot V_{ICF}, \quad \text{Eq. 18}$$

where R is the ratio of intracellular thymidine and nucleotide concentration to extracellular thymidine concentration. If there are differences in blood and extracellular thymidine concentration, these will affect the estimated range for V_{TdR}, as described by Equation 18.

The ratio R has been obtained for a variety of different tissue culture cell lines incubated in a medium containing labeled thymidine, in which the label concentration in the acid-soluble fraction (i.e., label not in macromolecules such as DNA) was measured and compared to the concentration in the incubating medium (*32,34,44*). R in these in vitro studies ranged from 1 to 50; however, in Hauschka's review of studies of human leukemic leukocytes, mouse L 929 cells and Novikoff hepatoma cells (*44*), cells incubated in physiologic concentrations of thymidine (1 μM or less) had uptake ratios (R) of 1–6. Assuming V_{ECF} and V_{ICF} of 0.3 and 0.65 ml/g, respectively (sum of extracellular space and intracellular space, exclusive of 0.05 ml/g blood volume), an R value of 6 in Equation 18 implies that V_{TdR} is equal to 4.2 ml/g. The theoretical lower limit for V_{TdR} is given by the case in which there is no cellular uptake (R = 0), in which case V_{TdR} would be 0.3. We have, therefore, assumed a range for V_{TdR} of 0.3–4 ml/g, which is consistent with our initial experience with the model.

It should be noted that V_{ECF} and V_{ICF} are likely to vary considerably, depending on tumor cellularity, and that such variability would affect the expected range for V_{TdR}. For example, in a highly cellular tumor, with V_{ICF} approaching 1 ml/g, V_{TdR} might potentially have a value as high as 6, the upper limit of the expected range for the intracellular-to-extracellular ratio R. Assumptions regarding V_{ICF} and V_{ECF} affect the range limits placed on the thymidine kinetic parameters, but they should not affect the accuracy of parameter estimates in most cases.

V_{TdR} can be related to model parameters by examining equilibrium conditions, in which case influx and efflux from the tissue thymidine compartment should be equal. This implies that K_{1t} times the blood thymidine concentration (influx rate) is equal to the efflux rate ($k_{2t} + k_{3t}$) times $[TdR]_{tis}$. V_{TdR} is therefore given by:

$$V_{Tdr} = \frac{K_{1t}}{k_{2t} + k_{3t}}. \quad \text{Eq. 19}$$

Recalling Equation 13, K_{TdR} is given by the following:

$$K_{TdR} = V_{TdR} \cdot k_{3t}. \quad \text{Eq. 20}$$

It should be noted that the experiments justifying a single, reversible tissue thymidine compartment with rapid turnover (Assumptions 2 and 3) were performed in highly proliferative tumors in animal models or in cell culture, where the turnover of the DNA precursor pool is rapid. These assumptions may be less well-justified in less rapidly proliferating tissues. For example, Spyrou and Reichard (*42*) found a smaller labeled nucleotide pool with slower turnover in G_0 cells compared to S-phase cells. Furthermore, it is likely that some or most of the label leaving the tissue compartment on the pathway represented by k_{2t} leaves as a labeled metabolite (likely thymine or DHT) rather than labeled thymidine, as assumed in the model. We will show later that, except under extremely rapid rates of tissue degradation and washout, this has little bearing on the estimation of thymidine incorporation into DNA.

Metabolite Compartment Set

Assumption 4: Metabolite Compartment Set. *Thymine, DHT and BUIB can be considered together in a single compartment set.*

The compounds in this compartment set result from the degradation of thymidine by thymidine phosphorylase (*1*). Studies have shown that most of the label in this group will be in the form of [^{11}C]DHT (*45*). Thymidine phosphorylase is a ubiquitous compound, found in many tissues, including tumors and platelets (*1,46,47*). Although tumors are likely to generate small amounts of thymine, DHT and BUIB, most will come from the blood as a result of degradative organs, such as the liver, and degradation by platelets (*1,47*).

There are only limited data on the transport and biodistribution of thymine, DHT and BUIB in vivo (*48,49*); however, because these compounds account for a relatively small fraction of the label in most tissues (5%–10% or less at 60 min), the approximation of a single tissue compartment will not greatly influence the estimation of thymidine incorporation parameters. Tissues in which these compounds are metabolized (e.g., the liver) will be a significant exception to this rule and may, therefore, not be characterized appropriately by the proposed model.

Assumption 5: Reversibility of Metabolite Transport. *Thymine, DHT and BUIB are reversibly transported to tissue; they are not trapped. They can therefore be modeled using a single tissue compartment with reversible transport, represented by K_{1m} (from blood to tissue) and k_{2m} (from tissue to blood).*

Studies in the literature (*1*) suggest that these compounds do not become bound in tissue except in organs, such as the liver, where they are degraded. Our own experience with labeled thymine confirms that the tracer is not concentrated in tissues that do not metabolize thymine (*49*). Therefore, this assumption should hold in tumor tissue but has not been experimentally validated in organs that metabolize thymine, such as liver, kidneys and, possibly, the spleen (*1*).

CO_2 Compartment Set

Assumption 6: Labeled CO_2 Transport. *Transport of labeled CO_2/HCO_3^- is reversible and can be described by a blood-tissue forward rate constant K_{1c} and a reverse rate constant k_{2c}.*

Experiments with labeled CO_2 in humans have shown that CO_2 is largely reversibly transported between blood and tissue and equilibrates according to tissue pH (*50,51*). K_{1c}/k_{2c} has been theorized to relate to tissue pH by the following equation (*51*):

TABLE 1
Thymidine Model Parameter Ranges and Starting Values

Parameter	Meaning	Units	Expected range		Starting value
			Minimum	Maximum	
K_{1t}	Thymidine capillary transfer rate constant	ml/min/g	0.050	0.300	0.200
K_{1t}/k_{2t}	Tissue thymidine volume	ml/g	0.30	4.00	2.00
k_{3t}	Tissue-to-DNA rate constant	min^{-1}	0.000	0.200	0.100
K_{1m}/K_{1t}	Relative metabolite capillary transfer	—	0.5	1.00	0.90*
K_{1m}/k_{2m}	Tissue metabolite volume	ml/g	0.10	1.00	0.50*
K_{1c}/K_{1t}	Relative CO_2 capillary transfer	—	0.50	1.00	0.70*
K_{1c}/k_{2c}	Tissue CO_2 volume	ml/g	0.20	1.20	0.80*
k_{3c}	CO_2 fixation rate constant	min^{-1}	0.000	0.012	0.005*
V_b	Tissue blood volume	ml/g	0.00	0.10	0.05*
Δt	Sampling site to image site time delay	min	−1	1	0

*Fixed value during optimization.

$$\frac{K_{1c}}{k_{2c}} = V_d \frac{1 + 10^{(pH_t - pK)}}{1 + 10^{(pH_p - pK)}}, \qquad \text{Eq. 21}$$

where pH_t and pH_p are the tissue and plasma pH values, respectively, V_d is the water volume of distribution in ml/g and pK is the apparent ionization constant for the CO_2/HCO_3^- buffer, equal to 6.12 (*51*). Assuming a V_d of 0.95 and a blood pH of 7.4, a tissue pH in the range of 6.5–7.5 implies a range for K_{1c}/k_{2c} of 0.2–1.2 ml/g.

Assumption 7: CO_2 Trapping. *A small amount of labeled CO_2 may become trapped in intracellular compounds, a process represented by the rate constant k_{3c}.*

Previous studies of labeled CO_2 have shown that the carbon label can become incorporated in a variety of molecules, some of which are macromolecules and trapped in tissues (*51–53*). The range of CO_2 fixation rates from studies of labeled CO_2 (*52–54*) provides bounds for k_{3c} of $0-0.012\ min^{-1}$.

Assumptions on the Relationship of the Compartment Sets

Assumption 8: Independence of Compartment Sets. *The thymidine, metabolite and CO_2 compartment sets are independent and driven by three separate components of the blood time-activity curves, each of which are measured by blood sampling and metabolite analysis.*

This assumption implies that tissues other than the tissue of interest are principally responsible for thymidine and metabolite degradation. It allows us to use three separate and independent compartment sets, greatly simplifying model calculations. This assumption is only justified for organs or tissues where local degradation is negligible, and so the blood is the sole source of thymine, DHT, BUIB and CO_2. Our calculations, based on blood metabolite concentrations measured in patients (*17*) and the expected rate constants for thymidine and metabolite blood-tissue transport, suggest that the rate of metabolite generation in most tissues should be small in comparison to the rate of transport from the blood. Also, because locally generated thymine, DHT and BUIB are not trapped in tissue, any locally generated molecules will quickly wash out into the blood. Our simulations, described here, show that the estimation of flux through the thymidine compartment set into DNA will not be affected by a modest level of local degradation. For the liver, where degradation of thymidine and metabolites is significant (*1*), this assumption may be violated.

Assumption 9: Relation of Blood-Tissue Transport Constants for Thymidine, Metabolites and CO_2. *The rate constants describing initial transport of thymidine, metabolites and CO_2, namely, K_{1t}, K_{1m} and K_{1c}, are fixed ratios of each other and are related to the capillary permeability of each tissue for each class of compound. These ratios should be similar in most tissues.*

This assumption represents a working hypothesis based on the fact that the delivery of the three classes of compounds will be closely related to blood flow, as well as our preliminary experience in animals (*unpublished data,* 1996). Because it ties the three K_1 rate constants together, it allows us to estimate a single K_1 with assumed values for the ratios to the other K_1 values, rather than three different K_1 values, reducing the number of free parameters in the model and improving the model's ability to estimate the common initial transport parameters.

It should be noted that in the brain, unlike other tissues, thymidine and thymine transport out of capillaries is limited by the blood-brain barrier, and the blood-tissue thymidine transport constant (K_{1t}) for thymidine and thymine is less than 3% of the water transport rate (*55*). CO_2 transport, however, is not significantly impeded (*50,51*). Thus, analysis of thymidine incorporation in brain tumors may require that the blood-tissue transport constants of the different compartment sets be considered independently.

MODEL PARAMETER ESTIMATION: MATHEMATICAL ANALYSIS AND SIMULATIONS

It would be unrealistic to expect to estimate all 10 model parameters from data of the quality obtained in a typical [^{11}C]thymidine imaging study. One approach would be to use three sequential injections of thymidine, thymine and CO_2 to measure parameters for thymidine and its labeled metabolites separately. Although this approach might be possible in animal validation studies, it is clearly impractical for patient imaging. The alternative and preferred approach is to explore the mathematical behavior of the model, to determine which parameters may be fixed during optimization without adversely biasing the estimation of parameters in the thymidine incorporation pathway and to assign values for the fixed parameters based on published data or experimental determination in a limited number of subjects.

We performed parameter sensitivity and identifiability analyses as previously described (*56–60*). These analyses investigate model behavior using calculations that incorporate the form of the model and a particular set of parameter values. Parameter values for these calculations were chosen to represent an actively proliferating tissue on the basis of the published data described above and our preliminary experimental data. Starting values are listed in Table 1, and ranges for the rate constants were discussed in the previous section. Our values for K_{1m}/K_{1t} and K_{1c}/K_{1t} are based on the initial results from animal studies.

Sensitivity calculations measure the degree to which a change in an individual input parameter results in a change in the output of the model. Parameters with high sensitivity are more likely to be estimated accurately than those with lower sensitivity (*56,57,60*). Sensitivity functions for each parameter k_α are time-varying quantities calculated as the partial differential of the model output [in this case, the total tissue time-activity curve, TAC(t)] with respect to k_α, normalized by TAC(t), and the value of k_α (*56,58,60*):

$$\text{Sens}_{k_\alpha}(t) = \frac{\partial \text{TAC}(t)/\text{TAC}(t)}{\partial k_\alpha/k_\alpha}. \qquad \text{Eq. 22}$$

The sensitivity function represents the fractional change in the total tissue time-activity curve at a given time t after injection as a result of a small change in the parameter.

Sensitivity functions for the parameters in the model were calculated using the modeling program Stella (High Performance Systems, Hanover, NH). Initial sensitivity analysis (data not shown) suggested reparameterization from K_1 and k_2 to K_1 and K_1/k_2 would improve identifiability for these parameters. Efflux parameters were, therefore, represented as tissue volumes (K_1/k_2) with units ml/g. To calculate sensitivity functions, parameter values representative of an actively proliferating tissue (starting values in Table 1) were used, and sensitivity values were estimated using a ±5% change in each parameter according to Equation 22.

Parameters with similar sensitivity functions cannot be estimated independently. Sensitivity function distinctiveness is described by identifiability analysis; identifiability is defined as the ability of a model parameter to be estimated independently of other model parameters. It is reflected by the correlation coefficients between pairs of model parameters, represented by the correlation matrix (*56*), which is the normalized inverse of the sensitivity matrix for the model, which, in turn, is approximated by the integrals over time of the products of the sensitivity functions (*56,57*):

$$\text{SM}_{k_\alpha k_\beta} = \int_0^{T_{end}} \text{Sens}_{k_\alpha}(\tau)\text{Sens}_{k_\beta}(\tau)d\tau, \qquad \text{Eq. 23}$$

where $\text{SM}_{k_\alpha} k_\beta$ is the sensitivity matrix element for the parameters k_α and k_β and T_{end} is the end of imaging time for a study beginning at injection (t = 0). Elements of this matrix represent the interaction of pairs of parameters in producing a change in the model output. The correlation matrix values range from −1 to 1; values close to ±1 indicate a high degree of correlation and suggest that the parameters cannot be estimated independently.

To estimate the correlation matrix, the sensitivity matrix was calculated by numerically integrating pairs of sensitivity functions for the parameter starting values listed in Table 1, using a trapezoidal approximation with a time step of 1 min. The sensitivity matrix was inverted and normalized using the spreadsheet program Excel 5.0 (Microsoft Corporation, Redmond, WA) to yield the correlation matrix.

Sensitivity and identifiability analysis suggested that only K_{1t}, K_{1t}/k_{2t}, k_{3t} and Δt could be estimated independently. We next investigated estimation of these parameters while tightly constraining the other parameters. As per Assumption 9, the K_1 values were set to fixed ratios of each other, whereas the metabolite tissue volume (K_{1m}/k_{2m}), CO_2 tissue volume, blood volume (V_b) and CO_2 trapping rate constant (k_{3t}) were held at fixed values based on the literature and our initial animal and patient results (Table 1). To determine the bias that might be introduced by these parameter constraints, we performed a series of simulations. Tissue time-activity curves were repeatedly generated using a typical set of thymidine, metabolite and CO_2 blood time-activity curves as input with numerical integration of the model's differential equations. The resulting time-activity curve was summed over time intervals to simulate noise-free dynamic PET data with scanning intervals beginning at injection of 4 × 20 sec, 4 × 40 sec, 4 × 1 min, 4 × 3 min and 8 × 5 min. Parameter values were set to the starting values listed in Table 1. During parameter estimation using the simulated data, K_{1m}/K_{1c}, K_{1m}/k_{2m}, K_{1c}/K_{1t}, K_{1c}/k_{2c}, k_{3c} and V_b were fixed to the starting values in Table 1; other parameters were estimated using the Levenberg-Marquardt optimizer (*56*) used in the P-Opt modeling software (*61*). For each of the fixed parameters, the tissue time-activity curve was regenerated over the range of parameter values in Table 1. The resulting bias in the estimated thymidine flux constant K_{TdR} was calculated so that the extent of bias resulting from fixing parameters during estimation could be determined.

To further characterize the ability of kinetic analysis to estimate individual parameters and the thymidine flux constant, we performed a series of simulations in which noise was added to the simulated tissue time-activity curves. Tissue time-activity curves were repeatedly generated as described above, with parameter values allowed to vary randomly over the ranges in Table 1. These values resulted in a range of K_{TdR} from 0 to 0.20 ml/min/g. Poisson noise was added to each point of the simulated tissue time-activity curves at a level that would be expected in a typical patient with a 555-MBq (15-mCi) injection of [^{11}C]thymidine and a 2-cm^3 region of interest in the center of a large tumor, taking isotope physical decay into account. Under these conditions, the 55- to 60-min data point in the simulated tumor time-activity curve obtained from the parameter starting values in Table 1 typically has a coefficient of variation of approximately 5%. Parameters were estimated by optimizing the model's fit to the simulated data. Although a variety of weighting functions were tried, simple equal weighting of each tissue time-activity point resulted in as good overall performance in estimating parameters pertinent to the thymidine compartment set as other more complex weighting schemes, as judged by the estimated versus true parameter correlation coefficients obtained in preliminary simulations. Optimizations were performed in two ways:

1. Estimating all parameters during optimization; and
2. Estimating only K_{1t}, K_{1t}/k_{2t}, k_{3t} and Δt while holding the other parameters at the fixed values listed in Table 1.

Note that, in simulated curve generation, all parameters were allowed to vary over their expected ranges, whether or not they were floated during optimization. In this way, both the random errors arising from curve noise and the systematic errors of assuming an incorrect fixed parameter were both considered.

In each case, the "true" parameter values which were used to generate each simulated curve were compared to the parameter values estimated in the optimization. In addition, the estimated flux constant (Eq. 13) was compared to the true value. For each parameter and for the thymidine flux constant, correlation coefficients and percentage biases were calculated for the estimated versus true values. For each simulation, 500 tissue time-activity curves were generated, which resulted in reproducible regression analyses for the simulations.

To test the impact on bias of local metabolism of thymidine in the tissue of interest, we added an additional pathway connecting the tissue thymidine and metabolite compartments (Fig. 4) to the model, described by a first-order rate constant, k_{met}. A family of noise-free tissue time-activity curves was generated using the parameter starting values in Table 1 and allowing k_{met} to vary from 0 (no local metabolism) to 0.4 min^{-1}, which is four times the value of the tissue-to-DNA rate constant, k_{3t}. For each curve, the

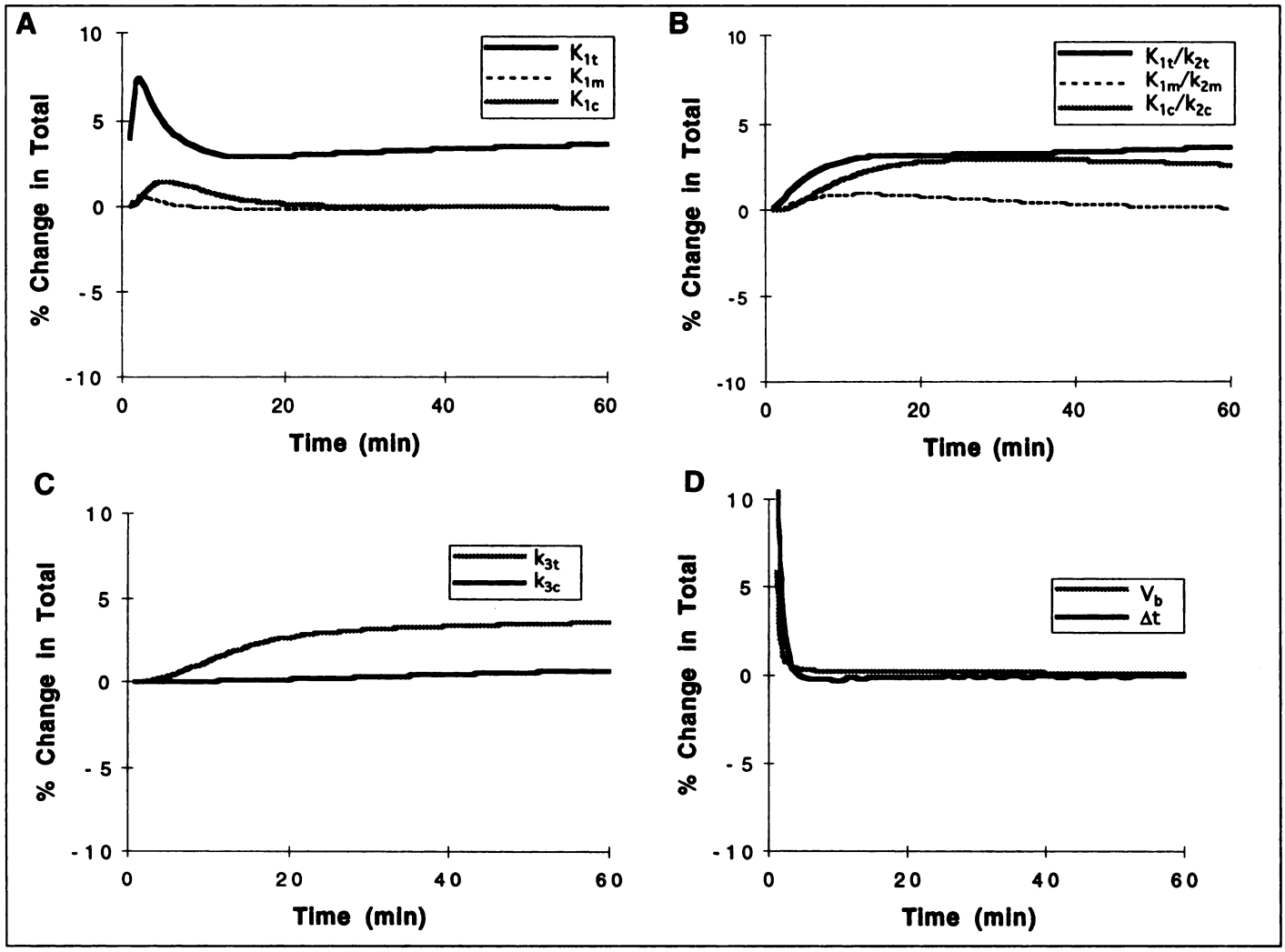

FIGURE 5. Sensitivity functions – percentage change in total tissue curve for a ± 5% change in the parameter. (A) K_1 parameters. (B) K_1/k_2 parameters. (C) k_3 parameters. (D) Blood sampling site to tissue site delay (Δt) and blood volume (V_b).

estimated K_{TdR} was compared to the true blood-tissue transfer constant, in this case given by:

$$K_{TdR} = \frac{K_{1t}k_{3t}}{k_{2t} + k_{3t} + k_{met}}. \qquad \text{Eq. 24}$$

Finally, to test the model's application to patient data, parameter estimation was performed on time-activity curves obtained from a patient with small-cell cancer of the lung, imaged just before and after 1 wk of chemotherapy. Arterial blood samples were obtained, and metabolite analysis of blood samples was performed as described previously (*17*). Dynamic PET images were obtained using a GE Advance tomograph (GE Medical Systems, Waukesha, WI) after the injection of 11.7 and 3.5 mCi of 2-[^{11}C]thymidine, prepared as described previously (*14*). Image data were time-binned in the same intervals used in the simulations. Tissue time-activity curves were obtained by drawing a 1.9-cm-diameter circular region of interest in the center of the lung mass on three adjacent 4.25-mm-spaced planes. Blood and tissue time-activity curves were used to estimate kinetic parameters from which the thymidine flux constant was calculated using Equation 13.

RESULTS

Sensitivity functions are plotted in Figure 5, and the correlation matrix is shown in Table 2. The sensitivity functions for K_{1t}/k_{2t} and K_{1c}/k_{2c}, k_{3t} and k_{3c} and V_b and Δt are qualitatively similar. The sensitivity function for K_{1m}/k_{2m} is shaped differently from the others, but it is small in magnitude because of the relatively small quantity of labeled metabolites other than CO_2 in the blood. The correlation matrix (Table 2) shows high correlation (correlation coefficient of approximately ±1) with at least one other parameter for all the CO_2 parameters and metabolite compartment tissue volume. There is also a high degree of correlation between V_b and Δt (delay), both of which predominantly affect the front end of the curve. These results suggest that only the thymidine compartment parameters and either V_b or Δt, but not both, can be independently estimated.

On the basis of the sensitivity function and correlation matrix analysis, we investigated the estimation of thymidine parameters with tight constraint on all other parameters except Δt. The results of simulations performed to determine the potential bias resulting from fixing parameters during estimation are summarized in Table 3. For each of the fixed parameters, the resulting worst-case percentage bias in the estimated thymidine flux constant (K_{TdR}) is listed. The coefficient of variation for K_{TdR} over the expected range of each fixed parameter tested, which reflects the average bias that might be expected, is also listed. The maximum bias in K_{TdR} as a result of parameter constraint was −32% to 21%, seen at the extremes of the expected range for the K_{1c}/k_{2c} parameter. The root mean-square bias of K_{TdR} over the range of parameter values tested was 0.3%–18%.

Correlation coefficients and percentage bias for the estimated versus true parameter relationships for simulated noisy tissue

TABLE 2
Parameter Correlation Matrix*

	K_{1t}	K_{1t}/k_{2t}	k_{3t}	K_{1m}	K_{1m}/k_{2m}	K_{1c}	K_{1c}/k_{2c}	k_{3c}	V_b	Δt
K_{1t}	1.00									
K_{1t}/k_{2t}	−0.36	1.00								
k_{3t}	−0.29	0.88	1.00							
K_{1m}	−0.44	−0.60	−0.65	1.00						
K_{1m}/k_{2m}	0.32	−0.96	−0.75	0.56	1.00					
K_{1c}	0.31	−0.96	−0.85	0.57	0.87	1.00				
K_{1c}/k_{2c}	0.30	−0.95	−0.98	0.66	0.84	0.93	1.00			
k_{3c}	0.34	−0.99	−0.92	0.63	0.95	0.94	0.97	1.00		
V_b	−0.10	0.12	0.12	−0.10	−0.11	−0.11	−0.12	−0.12	1.00	
Δt	0.00	0.00	0.00	0.04	0.00	0.00	0.00	0.00	−0.95	1.00

*Correlation coefficients of standard error values of pairs of model parameters. A value approaching ±1 indicates that these two parameters cannot be independently estimated.

time-activity curves are listed in Table 4. For both the optimizations in which all parameters were floated and those in which only a subset of parameters was floated, the correlation coefficients between true and estimated individual thymidine parameters were low, with the exception of the blood-tissue transfer constant (K_{1t}), which has $r > 0.9$. Despite the fact that the individual thymidine parameters are not well estimated, the errors in the individual parameters tend to compensate, resulting in a more robust estimate of K_{TdR} ($r = 0.90$ when all parameters were floated). On average, there was a slightly negative bias in the estimated flux constant (K_{TdR}) because of overestimation of activity in the CO_2 compartments. When only a subset of parameters were floated, the correlation of the estimated versus true K_{TdR} improved to $r = 0.94$, at the expense of slightly increased bias (−7% versus −4%).

Simulations in which local metabolism of thymidine was allowed resulted in errors in the estimation of individual parameters, as would be expected; however, the estimated flux constant (K_{TdR}) was within 1% of its true value, even at the highest level of local metabolism tested.

Patient tissue-time-activity curves and model fits are shown in Figure 6. Analysis of the pretherapy data resulted in an estimated thymidine flux constant of 0.060 ml/min/g, suggestive of a highly proliferative tumor. The patient was reimaged 1 wk later after one round of chemotherapy with cisplatin and etoposide. The post-therapy scan showed persistent activity at the tumor site; however, the time-activity curve was downsloping, and kinetic analysis estimated a thymidine flux constant of 0.009, which was only 15% of the initial flux constant. The patient went on to have a complete clinical response after completion of several months of chemotherapy.

DISCUSSION

One of the important determinants of tumor behavior is the rate of cellular proliferation. Changes in cell proliferation with therapy may provide an earlier indication of the success or failure of therapy (*5*) because cellular energetics often continues to be abnormally high after the cell has been doomed reproductively. Data on tumor proliferation have been obtained through in vitro analysis of biopsy specimens (*4,8*), which have also been tested as a predictor of response to cytotoxic chemotherapy agents (*9*). Although in vitro studies have demonstrated the potential utility of cell proliferation measurements, they are limited in their ability to characterize the heterogeneity of tumors and host-tumor interactions. PET imaging using labeled thymidine provides a tool capable of measuring proliferation in large tumors and/or multiple tumor sites, as well as monitoring response using serial studies. PET offers the possibility of quantitative estimates of thymidine incorporation into DNA, which should be useful in grading tumors and providing quantitative estimates of response to cytotoxic therapy. To quantify thymidine incorporation into DNA from PET images, however, requires a kinetic model that accounts for the behavior of the tracer and also labeled metabolites. Here, we have presented a model that retains the basic elements of thymidine incorporation into DNA and accounts for labeled metabolites. This model is based on known thymidine biochemistry in vitro, along with a limited number of studies in vivo (*2,3*), and our own preliminary in vivo experience in animals and patients (*11,16,19–21*).

The models presented here are lumped compartmental versions (i.e., simplifications) of more detailed physiologically realistic models (*62,63*) used to describe blood-tissue exchange

TABLE 3
Bias in Thymidine Flux Constant Resulting from Constraint of Parameters to Incorrect Values

Parameter	Fixed value	Expected range		Bias* (%)		Root mean-square bias† (%)
		Minimum	Maximum	At minimum value	At maximum value	
V_b	0.05	0	0.10	−3	3	2
K_{1m}/K_{1t}	0.9	0.5	1.0	1	0	0.3
K_{1m}/k_{2m}	0.5	0.1	1.0	−5	6	3.4
K_{1c}/K_{1t}	0.7	0.5	1.0	0	−1	0.4
K_{1c}/k_{2c}	0.8	0.2	1.2	−32	21	17.9
k_{3c}	0.005	0	0.012	−7	9	5.1

*Percentage bias in thymidine flux constant at minimum and maximum values of expected parameter range.
†Root mean-square percentage bias in thymidine flux constant over expected parameter range.

TABLE 4
Results of Simulations Using Tissue Time-Activity Curves with Noise Added

Parameter	Correlation*	Bias† (%)
All parameters estimated		
K_{1t}	0.93	2
K_{1t}/k_{2t}	0.54	−9
k_{3t}	0.56	−2
K_{TdR}	0.90	−4
Some parameters fixed‡		
K_{1t}	0.97 ± 0.01§	1 ± 2
K_{1t}/k_{2t}	0.63 ± 0.03	−12 ± 2
k_{3t}	0.73 ± 0.02	4 ± 1
K_{TdR}	0.94 ± 0.01	−7 ± 1

*Correlation coefficient for estimated versus true flux constant.
†Average percentage bias in estimated flux constant.
‡Only K_{1t}, K_{1t}/k_{2t}, k_{3t} and Δt were estimated; other parameters were fixed.
§Error ranges represent s.d. values of results from three different simulations.

and metabolism in preliminary analysis of thymidine kinetics and metabolite exchange (*20*). Nevertheless, they contain a large number of parameters to be estimated, considering the data obtained in a typical patient PET imaging study. We have performed a series of calculations and simulations designed to test the ability of such a complex model to accurately characterize thymidine kinetics from PET imaging data. Overall, our analysis suggests that it would be difficult to estimate all of the individual parameters in the model. Several of the model's parameters have significant covariance that, at the noise levels encountered in PET imaging data, results in significant errors in the estimation of individual parameters, especially those pertaining to labeled metabolites. Nevertheless, it is possible to make reasonable estimates of the overall flux of thymidine from the blood into DNA. Our analysis suggests that constraining some of the model's parameters during optimization does not overly bias parameter estimates and results in an improvement in the correlation of the estimated K_{TdR} with the true value. It is possible that such constraints might bias the thymidine flux estimate under extreme circumstances. For example, tissue pH affects K_{1c}/k_{2c}; therefore, flux estimates might be significantly biased by constraints on this parameter in the case of severely acidotic tumor tissue. An alternate approach that does not require such constraints is to estimate K_{TdR} graphically (*64*); however, this method only estimates the flux constant and provides no insight into the individual parameters.

Although thymidine flux can be estimated with reasonable fidelity, the estimation of individual parameters pertaining to thymidine kinetics is more problematic, even with highly constrained optimization. Our simulations show that it is possible to estimate delivery parameters (K_1) with good accuracy; however, labeled metabolites make it hard to reliably estimate the precursor pool size, represented by the thymidine distribution volume (V_{TdR}) and pool turnover into DNA, represented by k_{3t}. The ability to characterize tracer transport to tissue (K_{1t}) may be helpful in separating the effects of tracer delivery versus tissue proliferation. This may be important in tissues such as the brain, where there is limited thymidine delivery due to the blood-brain barrier and where it may be important to characterize both delivery and thymidine flux to separate blood-brain barrier changes from viable, proliferating tumor.

This article sets forth the biologic underpinnings of the model and describes analyses of its mathematical behavior and its

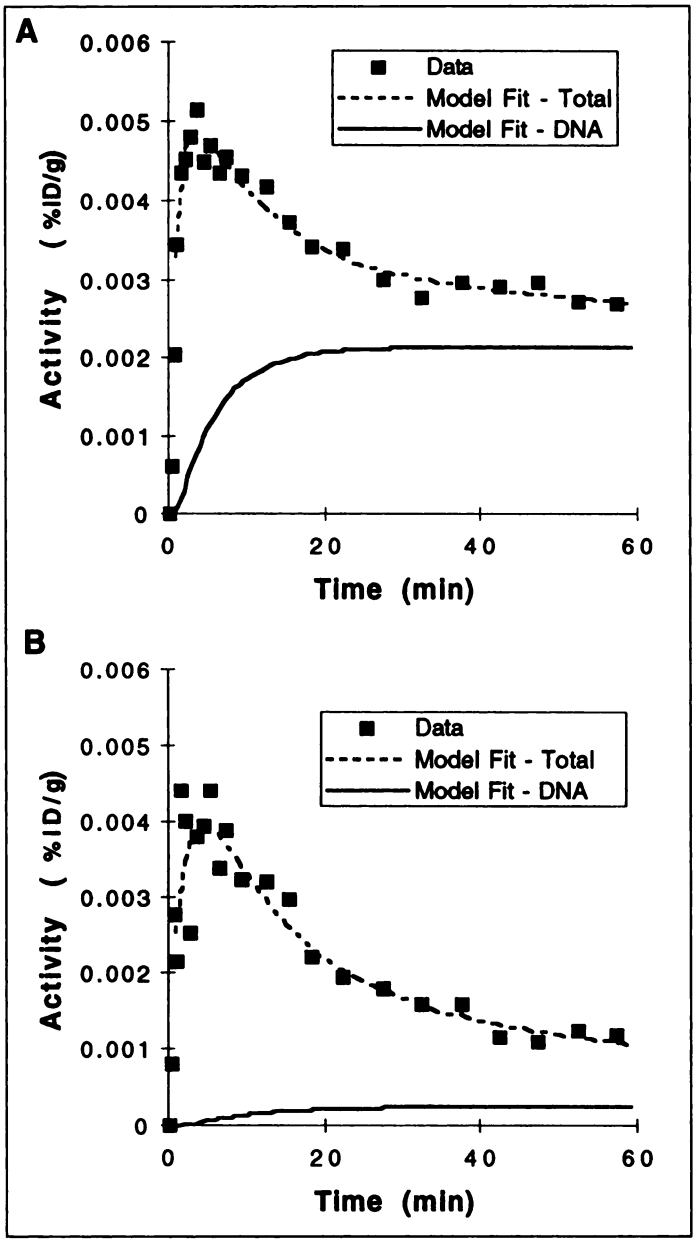

FIGURE 6. Model fits of data obtained from region of interest analysis of [^{11}C]thymidine studies of a patient with small-cell lung cancer studied using 2-[^{11}C]thymidine. Raw data (squares), model fit to the total curve (dashed line) and model prediction of activity in DNA (solid line) are shown. Tissue time-activity curves were obtained using 1.9-cm-diameter circular regions placed in the center of the tumor on three adjacent imaging planes. (A) Lung lesion pretreatment (11.7 mCi injected). (B) Same lesion after 1 wk of chemotherapy (3.5 mCi injected).

accuracy under the conditions encountered in PET imaging. The conclusions of our analyses are only as good as the validity of the assumptions underlying the model. Some of these assumptions are well supported by the literature; others, for example those regarding the behavior of thymine and related metabolites, have been less well studied. A series of animal and patient studies aimed at testing some of these assumptions and also testing the model's ability to estimate thymidine flux into DNA will be reported separately.

CONCLUSION

We have introduced a compartmental model for kinetic analysis of 2-[^{11}C]thymidine images to assess tissue proliferation by estimating thymidine flux from blood into DNA through the external pathway. This model accounts for the kinetic

behavior of thymidine as well as the labeled compounds that arise from its rapid metabolism. Initial analysis of the model suggests that it will be difficult to estimate individual parameters of the model, but that the model can provide robust estimates of thymidine flux into DNA.

ACKNOWLEDGMENTS

We thank Dr. Finbarr O'Sullivan, Dr. James Bassingthwaighte, Dr. Keith Kroll, Gary Raymond and Mark Muzi for helpful discussions, as well as Toby Lee, Kate Tewson and Trevor Olsen for technical assistance. This work was supported by National Institutes of Health (NIH) Grants CA42045 and CA39566, as well as the Mallinckrodt Fellowship of the Society of Nuclear Medicine (to David A. Mankoff). The model described here is a reduced form of models developed in the Simulation Resource for Circulatory Mass Transport and Exchange (NIH Grant RR1243).

APPENDIX

Glossary of Symbols

Symbol	Definition	Units
K_{1t}	Thymidine capillary transfer rate constant	ml/min/g
K_{1t}/k_{2t}	Tissue thymidine volume	ml/g
k_{3t}	Tissue-to-DNA rate constant	min^{-1}
K_{1m}/K_{1t}	Relative metabolite capillary transfer	—
K_{1m}/k_{2m}	Tissue metaolite volume	ml/g
K_{1c}/K_{1t}	Relative CO_2 capillary transfer	—
K_{1c}/k_{2c}	Tissue CO_2 volume	ml/g
k_{3c}	CO_2 fixation rate constant	min^{-1}
k_{met}	Local thymidine degradation rate constant	min^{-1}
K_{TdR}	Thymidine flux constant	ml/min/g
V_b	Tissue blood volume	ml/g
V_{TdR}	Thymidine volume of distribution	ml/g
V_{ECF}	Extracellular volume	ml/g
V_{ICF}	Intracellular volume	ml/g
V_d	Water volume of distribution	ml/g
$[TdR]_b$	Thymidine blood concentration	μmol/ml or μCi/ml
$[Met]_b$	Labeled non-CO_2 metabolite blood concentration	μCi/ml
$[CO_2]_b$	Labeled CO_2 blood concentration	μCi/ml
$[TdR]_{tis}$	Total thymidine and nucleotide tissue concentration	μmol/ml
$[TdR^*]_{tis}$	Labeled thymidine and nucleotide tissue concentration	μCi/ml
$[TdR]_{cell}$	Intracellular concentration of thymidine	μmol/ml
$[TdR]_{ECF}$	Extracellular concentration of thymidine	μmol/ml
$[TP]_{cell}$	Intracellular concentration of thymidine nucleotides	μmol/ml
$[TP]_{ECF}$	Extracellular concentration of thymidine nucleotides	μmol/ml
Δt	Sampling site to image site time delay	min
SR_{DNA}	DNA synthetic rate	μmol/min/g
$Flux_{TdR}$	Flux of thymidine into DNA via the external pathway	μmol/min/g
f_{ext}	Fraction of thymidine incorporated into DNA derived from external pathway	—
R	Ratio of intracellular thymidine and thymidine nucleotides to extracellular thymidine	—
TAC(t)	Tissue time-activity curve	μCi/g
$Sens_{k_\alpha}(t)$	Sensitivity function for the parameter k_α	—
$SM_{k_\alpha k_\beta}$	Sensitivity matrix element for the parameters k_α and k_β	—

REFERENCES

1. Cleaver JE. Thymidine metabolism and cell kinetics. *Frontiers Biol* 1967;6:43–100.
2. Tew KD, Taylor DM. The relationship of thymidine metabolism to the use of fractional incorporation as a measure of DNA synthesis in tissue proliferation. *Eur J Cancer* 1978;14:153–168.
3. Molnar P, Groothius D, Blasberg R, Zaharko D, Owens E, Fenstermacher J. Regional thymidine transport and incorporation in experimental brain and subcutaneous tumors. *J Neurochem* 1984;43:421–432.
4. Livingston RB, Ambus U, George SL, Freireich EJ, Hart JS. In vitro determination of thymidine-[H-3] labeling index in human solid tumors. *Cancer Res* 1974;34:1376–1380.
5. Livingston RB, Hart JS. The clinical applications of cell kinetics in cancer therapy. *Ann Rev Toxicol* 1977;17:529–543.
6. Kubota K, Ishiwata K, Kubota R, et al. Tracer feasibility for monitoring tumor radiotherapy: a quadruple tracer study with fluorine-18-fluorodeoxyglucose or fluorine-18-fluorodeoxyuridine, L-[methyl-^{14}C]methionine, [6-^{3}H]thymidine, and ^{67}Ga. *J Nucl Med* 1991;32:2118–2123.
7. Stewart PA, Quastler H, Skougaard MR, et al. Four-factor model analysis of thymidine incorporation into mouse DNA and the mechanism of radiation effects. *Radiat Res* 1965;24:521–537.
8. Tannock IF. Cell proliferation. In: Tannock IF, Hill RP, eds. *The basic science of oncology.* New York: McGraw-Hill; 1992:154–177.
9. Phillips RM, Bibby MC, Double JA. A critical appraisal of the predictive value of in vitro chemosensitivity assays. *J Natl Cancer Inst* 1990;82:1457–1468.
10. Christman D, Crawford EJ, Friedkin M, Wolf AP. Detection of DNA synthesis in intact organisms with positron-emitting [methyl-[C-11]] thymidine. *Proc Natl Acad Sci USA* 1972;69:988–992.
11. Shields AF, Larson SM, Grunbaum Z, Graham MM. Short-term thymidine uptake in normal and neoplastic tissues: studies for PET. *J Nucl Med* 1984;25:759–764.
12. Vander Borght T, Labar D, Pauwels S, Lambotte L. Production of [2-^{11}C]thymidine for quantification of cellular proliferation with PET. *Appl Radiat Isot* 1991;42:103–104.
13. Sundoro-Wu BM, Schmall B, Conti PS, Dahl JR, Drumm P, Jacobsen JK. Selective alkylation of pyrimidyl-dianons: synthesis and purification of ^{11}C labeled thymidine for tumor visualization using positron emission tomography. *Appl Radiat Isot* 1985;35:705–708.
14. Link JM, Grierson J, Krohn KA. Alternatives in the synthesis of 2-[C-11]-thymidine. *J Label Compd Radiopharm* 1995;37:610–612.
15. Martiat P, Ferrant A, Labar D. In vivo measurement of carbon-11 thymidine uptake in non-Hodgkin's lymphoma using positron emission tomography. *J Nucl Med* 1988;29:1633–1637.
16. Shields AF, Mankoff DA, Link JM, et al. Monitoring tumor response to chemotherapy with [C-11]-thymidine and FDG-PET [Abstract]. *J Nucl Med* 1996;37(suppl):67P.
17. Shields AF, Mankoff DA, Graham MM, et al. Analysis of 2-[C-11]-thymidine blood metabolites in PET imaging. *J Nucl Med* 1996;37:290–296.
18. Goethals P, van Eijkeren M, Lodewyck W, Dams R. Measurement of [methyl-carbon-11]thymidine and its metabolites in head and neck tumors. *J Nucl Med* 1995;36:880–882.
19. Shields AF, Lim K, Grierson J, Link J, Krohn KA. Utilization of labeled thymidine in DNA synthesis: studies for PET. *J Nucl Med* 1990;31:337–342.
20. Shields AF, Graham MM, Kozawa SM, et al. Contribution of labeled carbon dioxide to PET imaging of carbon-11-labeled compounds. *J Nucl Med* 1992;33:581–584.
21. Shields AF, Coonrod DV, Quackenbush RC, Crowley JJ. Cellular sources of thymidine nucleotides: studies for PET. *J Nucl Med* 1987;28:1435–1440.
22. Pelc SR, Appleton TC. Distribution of tritiated thymidine in various tissues. *Nature* 1965;205:1287–1289.
23. Goldspink DF, Goldberg AL. Problems in the use of [Me-[H-3]]thymidine for the measurement of DNA synthesis. *Biochim Biophys Acta* 1973;299:521–532.
24. Oliver JM, Paterson AP. Nucleoside transport. I. A mediated process in human erythrocytes. *Can J Biochem* 1971;49:262–270.
25. Wohlhueter RM, Marz R, Plagemann PGW. Thymidine transport in cultured mammalian cells, kinetic analysis, temperature dependence, and specificity of the transport system. *Biochim Biophys Acta* 1979;553:262–283.
26. Marz R, Wohlhueter RM, Plagemann PGW. Relationship between thymidine transport and phosphorylation in Novikoff rat hepatoma cells as analyzed by a rapid sampling technique. *J Supramol Struct* 1977;6:433–440.
27. Nottebrock H, Then R. Thymidine concentrations in serum and urine of different animal species and man. *Biochem Pharmacol* 1977;26:2175–2179.
28. Beaney R, Jones T, Lammertsma A, McKenzie D, Halnan K. Positron emission tomography for in-vivo measurement of regional blood flow, oxygen utilisation, and blood volume in patients with breast carcinoma. *Lancet* 1984:131–134.
29. Wilson CBJH, Lammertsma AA, McKenzie CG, Sikora K, Jones T. Measurements of blood flow and exchanging water space in breast tumors using positron emission tomography: a rapid and non-invasive dynamic method. *Cancer Res* 1992;52:1592–1597.
30. Goldman D, Bowen D, Gewirtz DA. Some considerations in the experimental approach to distinguishing between membrane transport and intracellular disposition of antineoplastic agents, with specific reference to fluorodeoxyuridine, actinomycin D, and methotrexate. *Cancer Treat Rep* 1981;65:43–56.
31. Taheri MR, Wickermasingthe RG, Hoffbrand AV. Alternative metabolic fates of thymine nucleotides in human cells. *Biochem J* 1981;194:451–461.
32. Yalowich JC, Goldman ID. Analysis of the inhibitory effects of VP-16-213 (etoposide) and podophyllotoxin on thymidine transport and metabolism in Ehrlich ascites tumor cells in vitro. *Cancer Res* 1984;44:984–989.
33. Taheri MR, Wickermasingthe RG, Hoffbrand AV. Functional compartmentation of DNA precursors in human leukaemoblastoid cell lines. *Br J Haematol* 1982;52:401–409.
34. Wohlhueter RG, Marz R, Graff JC, Plagemann PR. The application of rapid kinetic techniques to the transport of thymidine and 3-O-methylglucose into mammalian cells in suspension culture. *J Cell Physiol* 1976;89:605–612.
35. Leung KK, Visser DW. Characteristics of deoxythymidine transport and deoxythymidine kinase in 3T3 cells. *Biochem Med* 1976;16:127–137.
36. Colby C, Edlin G. Nucleotide pool levels in growing, inhibited, and transformed chick fibroblast cells. *Biochemistry* 1970;9:917–920.

37. Kuebbing D, Werner R. A model for compartmentation of de novo and salvage thymidine nucleotide pools in mammalian cells. *Proc Natl Acad Sci USA* 1975;72: 3333–3336.
38. Plagemann PGW, Erbe J. Thymidine transport by cultured Novikoff hepatoma cells and uptake by simple diffusion and relationship to incorporation into deoxyribonucleic acid. *J Cell Biol* 1972;55:161–178.
39. Sjostrom DA, Forsdyke DR. Isotope-dilution analysis of rate-limiting steps and pools affecting the incorporation of thymidine and deoxycytidine into cultured thymus cells. *Biochem J* 1974;138:253–262.
40. Nicander B, Reichard P. Dynamics of pyrimidine deoxynucleoside triphosphate pools in relationship to DNA synthesis in 3T6 mouse fibroblasts. *Proc Natl Acad Sci USA* 1983;80:1347–1351.
41. Reichard P. Ribonucleotide reductase and deoxyribonucleotide pools. *Basic Life Sci* 1985;31:33–45.
42. Spyrou G, Reichard P. Dynamics of the thymidine triphosphate pool during the cell cycle of synchronized 3T3 mouse fibroblasts. *Mutat Res* 1988;200:37–43.
43. Nederman T, Carlsson T, Kuoppa K. Penetration of substrates into tumor tissue. Model studies using thymidine and thymidine 5′-triphosphate in cellular spheroids. *Cancer Chemother Pharmacol* 1988;22:21–25.
44. Hauschka PV. Analysis of nucleotide pools in animal cells. In: Prescott DM, ed. *Methods in cell biology*, vol. 7. New York: Academic Press; 1974.
45. Goethals P, Lameire N, van Eijkeren M, Kesteloot D, Thierens H, Dams R. [Methyl-carbon-11]thymidine for in vivo measurement of cell proliferation. *J Nucl Med* 1996;37:1048–1052.
46. Usuki K, Norberg L, Larsson E, et al. Localization of platelet-derived endothelial cell growth factor in human placenta and purification of an alternatively processed form. *Cell Regul* 1990;1:577–596.
47. Shaw T, Smillie RH, Miller AE, MacPhee DG. The role of blood platelets in nucleoside metabolism: regulation of platelet thymidine phosphorylase. *Mutat Res* 1988;200:117–131.
48. Covey JM, Straw JA. Nonlinear pharmacokinetics of thymidine, thymine, and fluorouracil and their kinetic interactions in dogs. *Cancer Res* 1983;43:4587–4595.
49. Shields AF, Mankoff DA, Link JM, et al. Cardiac retention of labeled thymidine in humans and primates: a new metabolic pathway [Abstract]. *J Nucl Med* 1995; 36(suppl):143P.
50. Brooks DJ, Lammertsma AA, Beaney RP, et al. Measurement of regional cerebral pH in human subjects using continuous inhalation of [C-11]-CO_2 and positron emission tomography. *J Cereb Blood Flow Metab* 1984;4:458–465.
51. Buxton RB, Wechsler LR, Alpert NM, Ackerman RH, Elmaleh DR, Correia JA. Measurement of brain pH using [C-11]CO_2 and positron emission tomography. *J Cereb Blood Flow Metab* 1984;4:8–16.
52. Siesjo BK, Thompson WO. The uptake of inspired [C-14]-CO_2 into the acid-labile, the acid-soluble, the lipid, the protein and the nucleic acid fractions of rat brain tissue. *Acta Physiol Scand* 1965;64:182–192.
53. Lockwood AH, Finn RD. [C-11]-carbon dioxide fixation and equilibration in rat brain: effects on acid-base measurements. *Neurology* 1982;32:451–454.
54. Buxton RB, Alpert NM, Babikian V, Weise S, Correia JA, Ackerman RH. Evaluation of the [C-11]CO_2 positron emission tomographic method for measuring brain pH. I. pH changes measured in states of altered pCO_2. *J Cereb Blood Flow Metab* 1987;7:709–719.
55. Cornford EM, Oldendorf WH. Independent blood–brain barrier transport systems for nucleic acid precursors. *Biochim Biophys Acta* 1975;394:211–219.
56. Press W, Flannery B, Teukolsky S, Vetterling W. *Numerical recipes in C*. New York: Cambridge University Press; 1988:517–565.
57. Graham MM. Kinetic evaluation using sensitivity functions and correlation matrices-[Abstract]. *J Nucl Med* 1995;36:268P.
58. Casciari JJ, Graham MM, Rasey JS. A modeling approach for quantifying tumor hypoxia with [F-18]fluoromisonidazole PET time-activity data. *Med Phys* 1995;22: 1127–1139.
59. Vera DR, Krohn KA, Scheibe PO, Stadalnik RC. Identifiability analysis of an in vivo receptor-binding radiopharmacokinetic system. *IEEE Trans Biomed Eng* 1985;32:312–322.
60. Bassingthwaighte JB, Chaloupa JM. Sensitivity functions in the estimation of parameters of cellular exchange. *Fed Proc* 1984;43:181–184.
61. Graham MM. Parameter optimization programs for positron emission tomography data analysis [Abstract]. *J Nucl Med* 1992;33(suppl):1069.
62. Wangler RD, Gorman MW, Wang CY, DeWitt DF, Chan IS, Bassingthwaighte JB. Transcapillary adenosine transport and interstitial adenosine concentration in guinea pig hearts. *Am J Physiol* 1989;257:H89–H106.
63. Bassingthwaighte JB, Wang CY, Chan IS. Blood–tissue exchange via transport and transformation by endothelial cells. *Circ Res* 1989;65:997–1020.
64. Mankoff DA, Shields AF, Graham MM, Link JM, Krohn KA. A graphical analysis method to estimate blood-to-tissue transfer constants for tracers with labeled metabolites. *J Nucl Med* 1996;37:2049–2057.